Tactile Imaging System for Inclusion Size and Stiffness Characterization

Vira Oleksyuk, Firdous Saleheen, Yi Chen, and Chang-Hee Won
Email: {vira.oleksyuk, f.saleheen, yi.chen, cwon}@temple.edu
Department of Electrical and Computer Engineering, Temple University, Philadelphia, PA 19122, USA

***Abstract*—We developed Tactile Imaging System (TIS), which measures mechanical properties of tissue inclusions. The functional components of TIS include: a monochrome camera, a soft and transparent silicone probe, and an LED illumination circuit. The deformation of the soft TIS probe is used to evaluate size and compliance of inclusions, which is the inverse of elastic modulus. TIS algorithm development and testing were performed using a fabricated silicone tissue phantom with soft inclusions. We completed validation experiments for size and compliance estimation with TIS using the phantom. The results from these experiments suggest that TIS can be used for characterization of tissue inclusions.**

***Index Terms*— tactile sensing, size of inclusion, compliance of inclusion, tactile imaging.**

I. Introduction

Breast cancer is the second most common cause of cancer death in the USA [1], [2]. Studies show that stiffness of cancerous masses is higher than of benign masses [3], [4]. This knowledge fuels the development of many breast cancer screening methods.

Galea and Howe build a tactile imaging system, which utilizes multiple pressure sensors and a magnetic tracker. The authors reconstruct a tactile map of the experimental region [5]. Their device estimates tumors' size and elasticity. Another group of scientists, Egorov and Sarvazyan, work with a hand held breast imaging device. The outputs of the system include size, shape, hardness, strain, and mobility information about breast masses [6]. Both tactile imaging techniques take advantage of electromechanical pressure sensor technology. The number of pressure sensors defines the resolution of the system. A high resolution optical sensor, which is a charge coupled device (CCD) camera, is used in our Tactile Imaging System (TIS). The resolution of TIS is superior to the pressure sensors.

In this paper, we improved the original TIS design [7] by adding an external force gauge to measure the applied force and a potentiometer to control LED brightness. In addition, we propose a new LED circuit design to make LED performance more reliable—constant current for homogeneous illumination. To calibrate TIS and to develop its algorithm, we fabricated a custom silicone tissue phantom. The proposed new algorithm uses pixel number and intensity for size and compliance estimation of inclusions. We present the results from TIS phantom experiments in this paper.

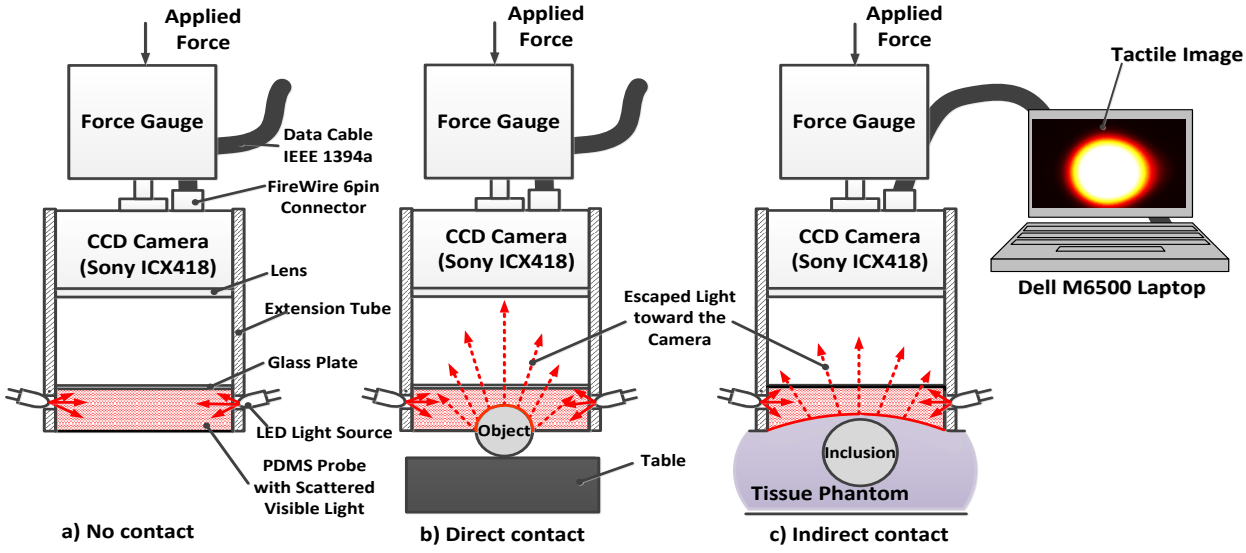

Fig. 1. Tactile Imaging System.

II. TIS Design And Principle

A. Sensing Principle and Hardware Design

Tactile Imaging System (TIS) utilizes the principle of total internal reflection of light. The light is trapped inside the soft silicone polymer [7]. Fig. 1 demonstrates the current TIS prototype. The polydimethyl-siloxane (PDMS) probe's dimensions are 20 mm × 23 mm × 14 mm. The elastic modulus of the material is 27 kPa. We use a Guppy F038 camera (Allied Vision Technologies, Exton, PA) with a Sony ICX418 CCD interlaced 1/2 inch sensor. The sensor's resolution is 8.4 µm × 9.8 µm. The tactile image size is 768 pixels × 492 pixels with 8 bit depth. The camera uses IEEE 1394A connection, and reaches the maximum frame rate of 30 fps. A Mark-10 Series 3force sensor (Mark-10, Long Island, NY) was mounted on the top surface of TIS to measure the applied normal force on the contact surface. The range of force gauge spans from 0 to 50 N (resolution is 1.0×10^{-3} N).

Fig. 1a shows TIS not in contact with a sample. In that case, there will be a dark tactile image on the laptop screen. Fig. 1b and Fig. 1c show TIS in direct contact with a sample, and in indirect contact with an inclusion region, respectively. The unique tactile image is generated for each of the cases.

B. LED Illumination Circuit

TIS illumination circuit utilizes four ultra-bright white LEDs (4 × 1500 mcd), and a 10 kΩ potentiometer to control brightness of the four LEDs. The diagram of the illumination circuit is shown in Fig. 2. This simple LED circuit design belongs to the first generation TIS. It was used for the data acquisitions described in this paper.

In order to increase the interrogation area of TIS optical probe and to keep uniform light intensity of TIS, we designed a new illumination circuit. The eight LEDs circuit is proposed for the second generation TIS, and will be experimentally tested in future work. Fig. 3 shows the new circuit schematics.

The brightness of the LEDs in TIS directly affects the acquired tactile images. It is very important to keep the uniformly distributed light intensities within the silicone probe during TIS image acquisitions. We designed a new lighting circuit with eight ultra-bright white, 3mm LEDs (8×4000 mcd). The circuit is powered by two Tadiran 3.6V coin cell lithium batteries.

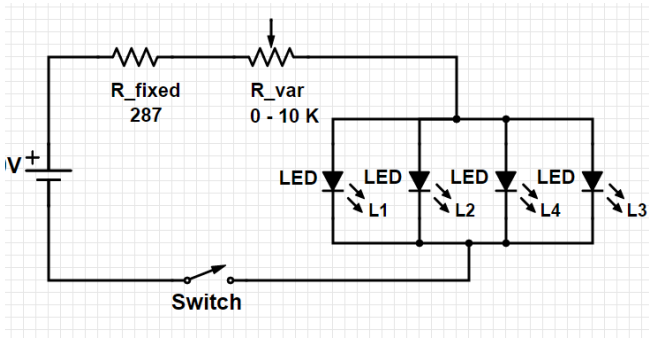

Fig. 2. Current TIS illumination circuit.

We connect the LEDs in series to supply the same current to each LED. This connection helps us to produce the LED light with uniform brightness. In addition, we use a constant current driver (LT1932 DC/DC LED Driver, ThinSOT Chip) to stabilize LED output over a range of input voltage, which helps to comply with the absolute maximum current rating of LED components. As a result, we obtain predictable and uniform luminous intensity and chromaticity from each LED. We use the pulse width modulation (PWM) dimming control instead of an analog 10 kΩ potentiometer to increase the battery life, and to improve the energy efficiency of the overall TIS design. Fig. 3 shows the schematic of the entire 8 LED circuit for the improved TIS. Due to the improved illumination circuit, the new generation of TIS will have an increased sensing area (40 mm × 40 mm). It will allow us to image larger samples and inclusions compared to the original TIS design.

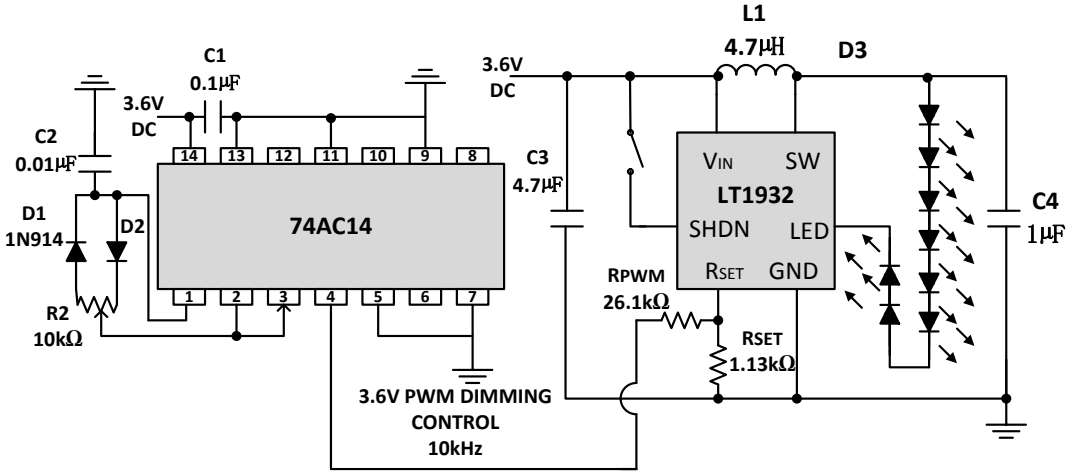

Fig. 3. Improved TIS illumination circuit.

III. METHODS

A. Inclusion Size Calculation

Here, we developed a 3D interpolation model (1) to estimate the size of spherical inclusions using TIS acquired data. Fig. 1 shows the geometry of the silicone probe in contact with an inclusion or tissue under applied normal force. We assumed spherical shape of the inclusions. The model captured interrelationships among the diameter of the inclusion, D, applied force, F, and the pixel number on the tactile image, N_p.

$$D(F,N_p)=\sum_{i=0}^{i=n}\sum_{j=0}^{j=m}p_{ij}F^iN_p^j, \tag{1}$$

where p_{ij} denotes the model coefficients.

Fig. 4 explains the size estimation method of TIS. From the number of pixels and force information, we estimate the size of the inclusion using this graph.

B. Inclusion Compliance Calculation

The ability of human skin and soft tissues to restore its shape after deformation suggests their elastic behavior [8]. The compression experiments with TIS mimic a conventional compression test procedure to determine tensile mechanical properties of inclusions [4], [9]. TIS measures compliance, by observing deformation of soft silicone probe during contact with a sample or inclusion. Young's modulus, E, is a stiffness measure of the material in the elastic region. It is calculated as stress (which is the applied normal force, F, divided by the contact area, A_C) divided by strain (which is the vertical deformation of the sample, dL, over the original vertical dimension of the sample, L). Fig. 5 illustrates TIS experimental setup. The compression surface in a conventional experiment with Instron testing machine is steel. A soft silicone probe layer is the compression surface of the TIS. This difference influences the output of these two methods. Due to the differences in the stiffness of the compression surface described previously, dL value (Fig. 5) for a stiff sample/inclusion in Instron test was smaller than the soft inclusion there. The TIS probe indentation change method measured strain from the pixel intensity change. This is inversely related to the stiffness of the target. TIS measures compliance, S_{TIS}, of the compressed tissues (2).

$$S_{TIS}=\alpha\cdot\frac{1}{E}, \tag{2}$$

where α is a scale factor determined empirically, and E denotes a slope of a stress-strain curve in the linear region.

We completed tactile experiments with the soft polymer spherical inclusions within our tissue phantom. We calculated the vertical stress value, $\sigma_z(k)$, for each tactile image k using (3).

$$\sigma_z(k)=\frac{F(k)-F_{ref}}{A_C}, \tag{3}$$

where $F(k)$ corresponds to the applied force. A_C is the area of contact between TIS and the experimental phantom (1134 mm^2). F_{ref} is the force that relates to the reference tactile image.

Next, the strain in vertical direction, ε_z for each TIS image was calculated as,

$$\varepsilon_z(k)=\frac{\Delta L}{L}=\frac{\left|I(k)-I_{ref}\right|}{I_{ref}}. \tag{4}$$

ΔL is the vertical change in size of the compressed sample, L is the initial vertical dimension of the sample, $I(k)$ denotes the k-th tactile image integrated intensity, and I_{ref} is the reference tactile image integrated intensity. The integrated intensity change of the tactile image relates linearly to the probe's indentation change [7], and we use it to measure the vertical size change of the sample.

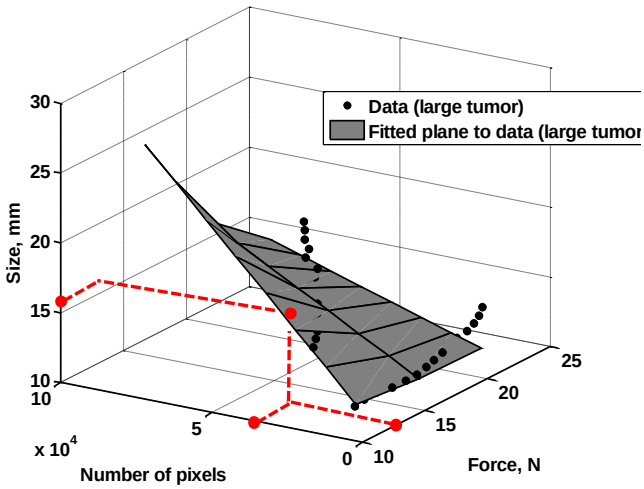

Fig. 4. Finding size using 3D interpolation.

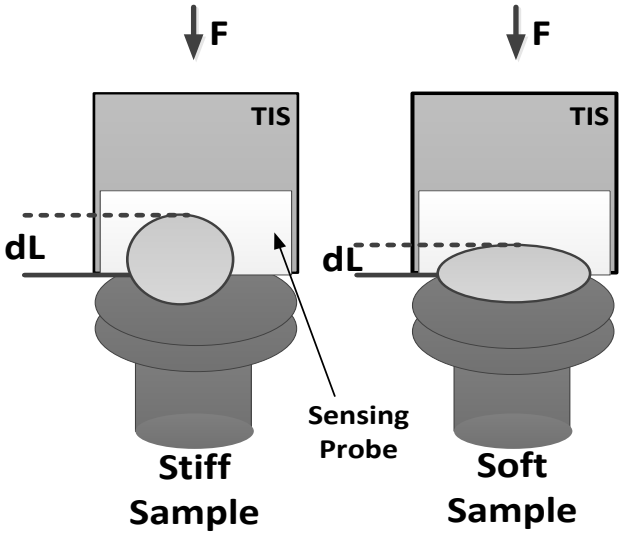

Fig. 5. Compression experiment.

IV. PHANTOM

A. Phantom Development

We fabricate artificial human breast tissue and tumor phantoms to validate TIS algorithms. Even though there are many approaches to develop experimental phantoms, the phantoms making procedures for the mimicking elastic properties of the tissue are not well established. The tissue phantoms described in the literature are application specific and were not well aligned with our needs. Researchers use different materials to fabricate phantoms. Some prefer a gelatin mixture for their experimental tissue phantoms, and they often mimic tissue acoustic properties [10], [11]. However, gelatin phantoms showed low performance in repeatable compression tests in our lab. PDMS is often used for the phantom fabrication. Egorov and Sarvazyan do not use soft inclusions, yet they have many hard spheres implanted at the varying depth within soft silicone [6]. We also use PDMS material to make our inclusions, yet we vary their stiffness. Other researchers prefer polyvinyl chloride (PVC) material for their tissue mimicking [12]. We use PVC for our tissue phantom fabrication. Beccani *et al.* do not change stiffness of the inclusion. The constant stiffness of the tumors was not sufficient to test TIS algorithms. We decided to fabricate a tissue phantom from PVC material because it could sustain multiple TIS compressions without breaking.

Our tissue phantom had four PVC layers and multiple soft PDMS inclusions, which mimicked tumors of varying size and stiffness.

B. Phantom Characteristics

A tissue phantom and soft inclusions are made to develop and test TIS algorithms. The PVC tissue phantom mimicked human breast tissues and was composed of multiple layers, such as skin, depth, intermediate, and base layers. The base layer (~125 kPa) corresponded to deep muscle and fibrous tissue. The intermediate layer (~10 kPa) mimics fatty tissue of the breast. The depth layer allowed us to change the depth of the inclusions during tactile experiments. The skin layer (~80 kPa) corresponds to human skin. The elastic properties of the layers are supported in the literature [13], [11], [12].

TABLE I
PHANTOM LAYERS

Layer	Composition	Height, mm	Young's modulus, kPa
Base	Regular Liquid Plastic	15	124
Intermediate	Regular Liquid Plastic : Softener = 1:1	10, 16	7
Depth	Regular Liquid Plastic : Softener = 1:1	2, 4, 6, 8, 10	7
Skin	Super Soft Liquid Plastic	<1	78

TABLE II
SPHERICAL INCLUSIONS

Material	Purpose	Size, mm	Base : Curing Agent	Young's modulus, kPa
Polyacrylo nitrile (Acrylic)	Size Algorithm	8.02 8.80 9.85 11.85 13.78 15.47	N/A	200,000 ~ 390,000
Polydimethyl siloxane (PDMS)	Compliance Algorithm	16.00	1:2 1:3 1:4 1:5 1:7.5 1:10 1:20	68 134 193 236 308 355 466

Table I presents the phantom description in detail. The elastic moduli of fabricated tissues and spherical phantoms were measured using Instron 4442, Instron Inc. The preload for all samples was 0.2 N. Crosshead speed was 300 mm/min.

We used two kinds of inclusions for our experiments: the hard spheres of different size and constant stiffness (used for the size algorithm), and the soft PDMS spheres of different stiffness and constant size (used for elasticity estimation algorithm). Table II gives a greater description of the inclusions.

We combined all four layers and inclusions for the tactile experiments. In the glass container, the base layer was the lowermost layer. We placed the intermediate layer over the base layer. One inclusion at a time was inserted with the small incision in the middle of the intermediate layer. Later, we covered the inclusion region with one depth layer and the skin layer. Fig. 6 shows the phantom components and illustrates how the layers were aligned for the experiments.

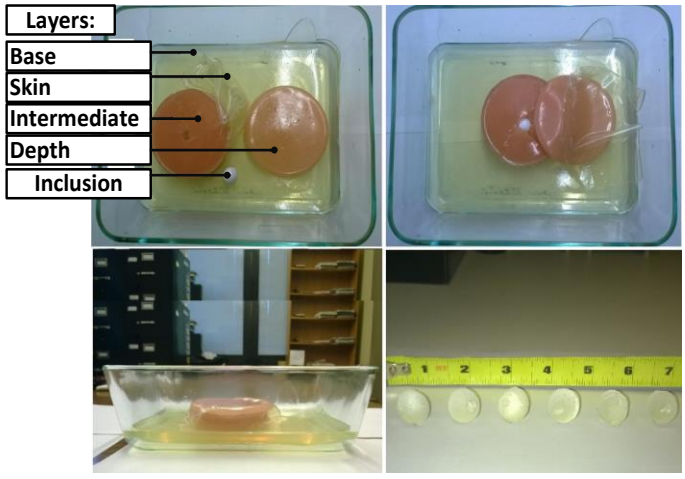

Fig. 6. Tissue phantom and spherical inclusions.

V. Results

A. Image Processing

We preprocessed all tactile images prior to mechanical properties estimation. The regions with increased intensity of pixels indicated deformation of the waveguide and were used for the calculation. From the histograms of many TIS experimental images, we set the intensity level threshold at 30 for segmentation. This procedure allowed us to differentiate the regions of interest from the background and to continue with calculations.

B. Size Calculation

We estimated diameters of the inclusions using information about the applied forces and the number of pixels at tactile images. Multiple interpolation surfaces were developed based on equation (1), which is a general case. The form and order of polynomial (7) were chosen empirically to align with TIS results.

$$D(F, N_p) = p_{00} + p_{10}F + p_{01}N_p + p_{20}F^2 + p_{11}FN_p + p_{30}F^3 + p_{21}F^2N_p \quad (7)$$

We developed two types of the interpolation models to correlate with size and depth changes of inclusions. The first type corresponded to the large inclusions. The large inclusions were of 11.85 mm and 15.47 mm in diameter. Another type corresponded to the small inclusions, with 8.02 mm and 9.85 mm in diameter. The interpolation surfaces were computed for six depth layers (0, 2, 4, 6, 8, 10 mm). The calculation of the p_{ij} parameters sets completed the 3D interpolation model estimation. Using this model, we calculated the size of the inclusions from the pixel information on tactile images and the force information from the force gauge. The graphical representation of the size estimation using 3D interpolation method is shown in Fig. 4.

We had multiple interpolation surfaces for different depths. The interpolation surface in Fig. 4 corresponds to the large inclusions set and 10 mm depth. The choice of a particular 3D interpolation surface was based on the approximated depth and size of the inclusions.

Diameter and depth of the inclusions was varied during TIS size experiments, using three depth layers (2, 6, 10 mm) and the fabricated PDMS spheres (Table II). There were three trials for each experiment to decrease the influence of the possible experimental errors. Table III presents the results for TIS size estimation.

C. Compliance Calculation

For the stiffness evaluation experiments, we measured compliance of the inclusions in the tissue phantom by mimicking the elastic modulus estimation method of Instron [4], [9]. TIS is attached to the loading machine, and the phantom container was placed on the loading machine's base. TIS acquisitions were done directly on a top of the phantom's inclusion region. The step-wise force was applied to TIS towards the phantom in the range from 0 to 26 N with small increments. The experimental images and force information were saved. For compliance calculations, we utilized PDMS spherical inclusions of different stiffness, described in Table III. The true stiffness of the spherical samples were found in compression experiments using Instron 4442 as 68 kPa, 193 kPa, and 466 kPa, respectively. All compliance experiments were completed with 4mm depth layer. Fig. 7 demonstrates the stress-strain curves for the three inclusions. We noticed the slope decreases for the stiffer sample (PDMS 1:20) relative to the slopes for the softer samples. We estimated compliance of PDMS inclusions by inverting the TIS Young's modulus results and multiplying it by a scale factor of 1000. Table IV shows the results of compliance calculation. Sample 1 had the smallest elastic modulus, and sample 3 had the highest elastic modulus. We see from Table IV that the calculated compliance value decreased with the decrease of the sample's stiffness.

TABLE III
Size Experiment Results

Depth, mm	Sample Material	Fabric. Ratio	True Young's modulus, kPa	Calc. Size, mm	Size Error, %
2 mm	PDMS	1:3	134	15.08	3.95
		1:5	236	14.85	7.30
		1:10	355	15.83	0.81
		1:20	466	14.58	10.72
	Acrylic	n/a	200,000-390,000	15.38	0.77
6 mm	PDMS	1:3	134	12.71	19.04
		1:5	236	12.65	21.04
		1:10	355	12.81	19.74
		1:20	466	12.80	21.62
	Acrylic	n/a	200,000-390,000	13.31	14.13
10 mm	PDMS	1:3	134	16.59	5.67
		1:5	236	16.84	5.12
		1:10	355	16.10	0.88
		1:20	466	16.41	0.49
	Acrylic	n/a	200,000-390,000	16.27	4.97

TABLE IV
Compliance Experiment Results

Sample #	Stiffness, kPa	Compliance (S_{TIS}), kPa^{-1}
1	68	17
2	193	22
3	466	48

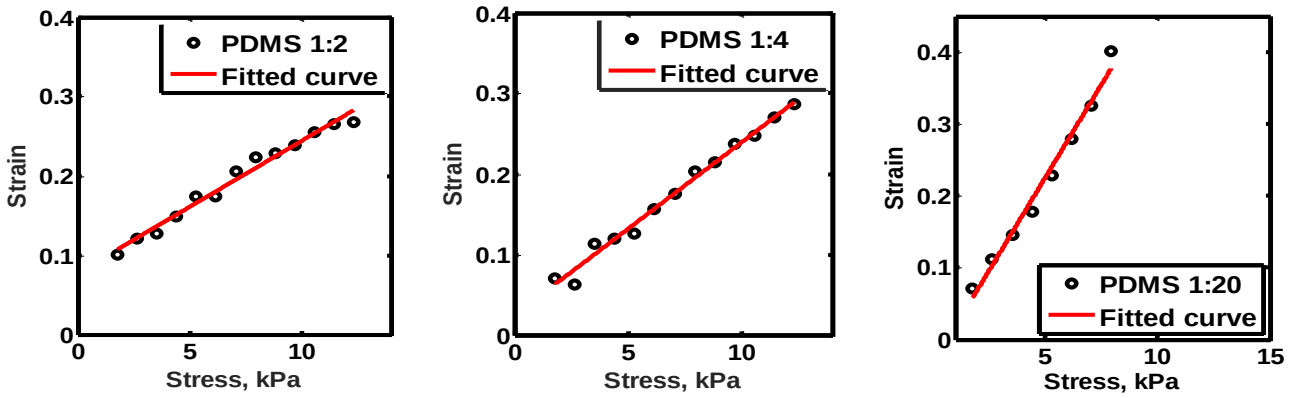

a) b) c)

Fig. 7. Stress-strain relationships for the phantom experiments. (a) soft inclusion, (b) medium stiffness inclusion, and (c) stiff inclusion.

VI. Discussion and Conclusions

We proposed a method for mechanical properties estimation of inclusions. The developed Tactile Imaging System (TIS) and its algorithm can estimate size and compliance of inclusions. Size of inclusions is estimated using 3D interpolation method. Compliance of inclusions is estimated from their indentation into silicone probe under TIS compression. We developed a custom silicone phantom with soft inclusions. The phantom was used to test TIS algorithms.

Our results showed that TIS is capable of measuring size and stiffness of the inclusions. The errors of inclusion size estimation ranged from 0.49% to 21.62%, and showed tendency to increase with the increase of inclusion's depth. The compliance experimental results demonstrated correlation of the TIS output with the true Young's modulus values of the inclusions.

Acknowledgement

This material is based upon work supported by the National Science Foundation under Grant No. DGE-1144462, and the Tobacco Formula Fund of Pennsylvania Department of Health.

We are thankful to Dr. Rouzbeh Tehrani and Gangadhar Andaluri, Civil & Environmental Engineering Department, Temple University for letting us use their lab facilities. We thank Anthony Lowmen, PhD, and Samuel Laurencin from the College of Engineering, Rowan University, NJ for letting us use their instruments.

References

[1] I. Ferlay, M. Soerjomataram, R. Ervik, S. Dikshit, C. Eser, M. Mathers, D. Rebelo, D. Parkin, Forman, and F. Bray, "Cancer incidence and mortality worldwide," Lyon, France, 2012.

[2] "Cancer facts and figures 2015, What are the key statistics about breas oft cancer?," Atlanta, GA, 2015.

[3] P. Wellman, E. P. Dalton, and D. Krag, "Tactile Imaging of Breast Masses," *Arch. Surg.*, vol. 136, no. 2, pp. 204–208, 2001.

[4] T. Krouskop, T. Wheeler, F. Kallel, B. Garra, and T. Hall, "Elastic Moduli of Breast and Prostate Tissues Under Compression," *Ultrason. Imaging*, vol. 20, no. 4, pp. 260–274, 1998.

[5] A. M. Galea and R. D. Howe, "Tissue stiffness from tactile imaging," *Proc. Second Jt. 24th Annu. Conf. Annu. Fall Meet. Biomed. Eng. Soc. Engineering Med. Biol.*, vol. 2, pp. 935–936, 2002.

[6] V. Egorov and A. P. Sarvazyan, "Mechanical imaging of the breast," *IEEE Trans. Med. Imaging*, vol. 27, no. 9, pp. 1275–1287, 2008.

[7] J. H. Lee and C. H. Won, "The tactile sensation imaging system for embedded lesion characterization," *IEEE J. Biomed. Heal. Informatics*, 2013.

[8] A. Kerr, *Introductory Biomechanics*. Edinburg: Churchill Livingstone, 2010.

[9] "Instron Model 4400 Universal Testing System Operator's Guide," Norwood, MA, 1995.

[10] T. J. Hall, M. Bilgen, M. F. Insana, and T. A. Krouskop, "Phantom materials for elastography," *IEEE Trans. Ultrason. Ferroelectr. Freq. Control*, vol. 44, no. 6, pp. 1355–1365, 1997.

[11] I. Cespedes, J. Ophir, H. Ponnekanti, and N. Maklad, "Elastography: Elasticity Imaging Using Ultrasound with Application to Muscle and Breast In Vivo," *Ultrason. Imaging*, vol. 15, no. 2, pp. 73–88, 1993.

[12] M. Beccani, C. Di Natali, L. J. Sliker, J. A. Schoen, M. E. Rentschler, and P. Valdastri, "Wireless tissue palpation for intraoperative detection of lumps in the soft tissue," *IEEE Trans. Biomed. Eng.*, vol. 61, no. 2, pp. 353–361, 2014.

[13] A. M. Galea, "Mapping Tactile Imaging Information: Parameter Estimation and Deformable Registration," Harvard University, 2004.